Ultrashort-Pulse Laser Ellipsometric Pump-Probe Experiments on Gold Targets

Hitoki Yoneda,[1] Hidetoshi Morikami,[1] Ken-ichi Ueda,[1] and Richard M. More[2]
[1]*Institute for Laser Science, University of Electro-communications, Chofu, Tokyo 182-8585, Japan*
[2]*National Institute for Fusion Science, Toki, Gifu 509-5292, Japan*
(Received 25 February 2003; published 14 August 2003)

Ultrashort-pulse laser pump-probe ellipsometry has been performed on gold targets at intensities 2×10^{12}–5×10^{13} W/cm^2. We measured time-resolved p- and s-polarized reflectivity (r_p and r_s) and the s-p phase difference (δ). When plotted as $Y = [2|r_s||r_p|\sin(\delta)]/(|r_s|^2 + |r_p|^2)$ versus $X = |r_p|^2/|r_s|^2$, the experimental data follow approximately the same curve in X-Y space, even for different pump intensities. Although the input energy density is about 40 eV/atom and the plasma expansion is rapid (up to 10 km/sec), our data are consistent with a partially transparent blowoff having an atomic polarizability $(-1.75 + 0.2i) \times 10^{-24}$ cm^3. We attribute this behavior to recombination in the expanding plasma. The Saha equation predicts recombination and formation of negative ions and a low density of free electrons in the low-density vapor, and solutions of the Maxwell equations approximately reproduce the data.

DOI: 10.1103/PhysRevLett.91.075004 PACS numbers: 52.38.–r, 52.50.Jm

Pump-probe reflectometry is now widely used for study of ultrafast phenomena in condensed matter. Similar investigations of laser-heated materials at high energy density, such as the study of the resistivity of hot dense matter [1,2], may open a new field of research and give useful information about the transition between solid-state and plasma physics.

To fully understand the optical properties of a heated target, it is necessary to measure both reflectivity and phase. Zheludev [3] and Dhanjal [4] measured small changes of reflectivity and phase by metal surfaces for pump irradiance $\sim 10^9$ W/cm^2. They used pulses from an ultrashort-pulse mode-locked oscillator so they could detect reflectivity and phase changes of 10^{-6} using a lock-in amplification technique. The metal was heated to the melting temperature. To explore higher temperatures, Blanc *et al.* [5] proposed frequency domain interferometry to detect phase shifts of s- and p-polarized probe pulses. Grimes *et al.* [6] used this method to measure hydrodynamic expansion from solid targets.

Here we report results from a new type of pump-probe measurement with an ultrashort-pulse laser. Figure 1 shows a schematic drawing of the experimental setup. The probe beam is a 745 nm, 120 fs Ti:sapphire laser pulse and the heat pulse is a frequency-tripled 248 nm pulse having 300 fs pulse duration, amplified by a Kr*F excimer laser amplifier. The pump beam has normal incidence and the probe beam arrives at 64° from the target normal. The incident probe beam is polarized at 45° so the s- and p-polarized components are equal. The pump focal spot has 10 μm diameter and the probe beam spot is a 4 μm by 6 μm ellipse.

A four-detector photopolarimeter [7] is used to determine reflectivity and phase for each polarization. We study two ratios of polarization components denoted $X = I_1/I_2$ and $Y = (I_3 - I_4)/(I_3 + I_4)$. X is the ratio of p- and s-polarization ($I_1/I_2 = |r_p|^2/|r_s|^2$), and Y is $(I_3 - I_4)/(I_3 + I_4) = [2|r_s||r_p|\sin(\delta)]/(|r_s|^2 + |r_p|^2)$, which depends on the phase difference between s- and p-polarization reflection (r is the reflected wave amplitude). Because of dielectric-coated mirrors between target and detector and differences of detector sensitivity, a residual polarization is produced in the measurement system. Therefore, each detector was calibrated using data for cold gold before starting the experiments. The ratios X and Y are much less sensitive to fluctuations of the probe beam intensity than the detector signals I_j. Typical detection sensitivity is 5×10^{-3} rad for the phase difference of p- and s-polarized light and the corresponding uncertainty in the optical parameters n and k were ± 0.015 and ± 0.05, respectively. The measured signals are averages over the probe pulse duration and small focal-spot area (which is about 20% of the heated area).

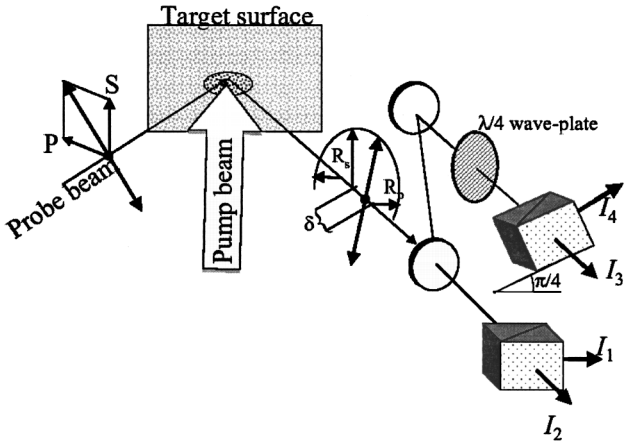

FIG. 1. Schematic drawing of experimental setup for 4-detector ellipsometric pump-probe measurement.

A 500 nm thick gold layer on glass was irradiated with the pump beam at peak intensities of 2×10^{12}–5×10^{13} W/cm^2. The target was rotated so that each pump pulse encountered a fresh surface. An oblique-incidence cw laser was used for monitoring the target surface position and the deviation signal was fed back to the translation stage to keep proper alignment between pump and probe beam.

Figure 2 shows typical time dependence of the ratios X, Y. Before arrival of the pump laser pulse, the ratios are the constant parameters for cold gold. At the probe laser frequency, solid gold shows the normal metallic (Drude) behavior, with an electron effective mass of 1.33 times the vacuum electron mass. After arrival of the heat pulse, both X and Y decrease. During the pump pulse, the target surface temperature is rapidly rising. We usually observe an inflection point where the changes seem to pause. (In the lower intensity case of Fig. 2, this point is at $t =$ 200–300 fs.) If the target is treated as a homogeneous metal with a complex refractive index $n' = n + ik$, then the n and k values can be extracted with the Fresnel formulas. The calculated real part of ε $(= n^2 - k^2)$ remains constant from the start of heating to the inflection point, and the imaginary part of ε $(= 2nk)$ increases with time. These observations are consistent with a Drude law, $\varepsilon(\omega) = 1 - [\omega_p^2\tau^2/(1 + \omega^2\tau^2) + i(\omega_p^2\tau/\omega)/(1 + \omega^2\tau^2)]$, with a constant electron plasma frequency ω_p and with the damping $(1/\tau)$ rising with temperature. For different pump intensities, the value of $2nk$ at the inflection point is about the same (8–10). This point probably corresponds to the boiling point. After the inflection point, the Drude formula cannot be used because strange parameters are required to fit the experimental results. After boiling, of course, target expansion must also occur.

To analyze the hot material, we plot $Y(t)$ against $X(t)$. Figure 3 shows the data trajectories for seven sets of experiments. Each data point represents a ~30 shot average and the total number of laser shots is ~3000. The trajectories divide into two groups. For the lower intensity ($I \sim 2 \times 10^{12}$ W/cm^2), the data points move from $(X, Y) = (0.9, 0.7)$ to $(0.6, 0.5)$ while in the higher intensity cases ($I \sim 3 \times 10^{13}$ W/cm^2) the trajectories reach $(0.2, 0.1)$. In both cases these changes occur in about 1 psec. After reaching their minimum point, the (X, Y) trajectories return to the initial point by various routes. In the lowest intensity case, the return almost retraces the heating path. For higher intensities, the return passes below the heating route. To avoid complexity in viewing Fig. 3, only one return path is indicated with hatching.

These trajectories have a remarkable feature. Even though the irradiation intensity and final turning point vary and the time derivatives of $X(t)$, $Y(t)$ vary, *all the trajectories follow approximately the same curve in X, Y space.* For still higher intensity ($> 4 \times 10^{13}$ W/cm^2), the experimental trajectory falls below this *unique* track.

To understand these observations, we solve the Maxwell equations with various models for the target conditions. In the calculations, the evaporated gold is taken to form a one-dimensional rarefaction plasma. The expansion is planar during the first picosecond

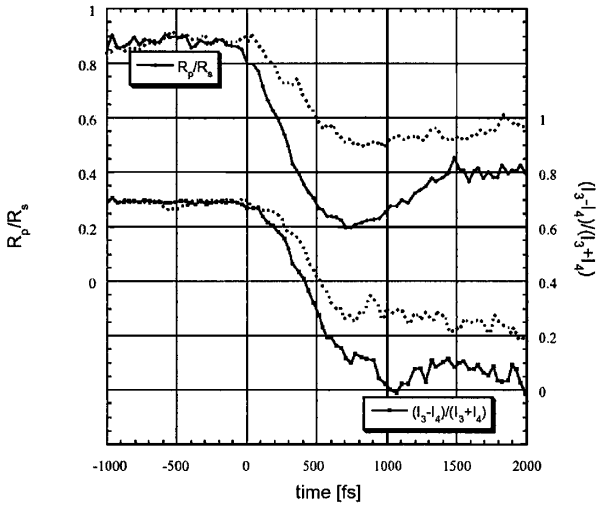

FIG. 2. Typical time dependence of $I_1/I_2 = R_p/R_s = |r_p|^2/|r_s|^2$ and $(I_3 - I_4)/(I_3 + I_4) = [2|r_s||r_p|\sin(\delta)]/(|r_s|^2 + |r_p|^2)$. The arrival time of the pump beam is near $t = 0$. The solid line denotes a higher intensity case ($I = 2 \times 10^{13}$ W/cm^2) and the dotted line denotes a lower intensity ($I \sim 7 \times 10^{12}$ W/cm^2). In the case of lower irradiance, there is an "inflection point" observed during the heating process ($t = 200$–300 fs). The detector data are calibrated to match the known properties of cold gold at an early time.

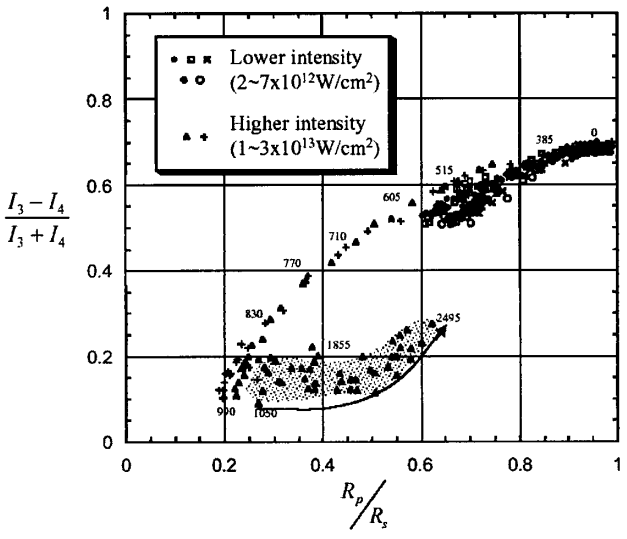

FIG. 3. Ellipsometry trajectories of gold targets. These X, Y trajectories can be divided into two groups. The low intensity shots stop at $X \sim 0.6$ and the high intensity shots reach $X \sim 0.2$. Although the pump intensities are different, the trajectories follow approximately the same curve in X, Y space. The number inside the figure gives the time from start point in femtoseconds for one trajectory (triangle dot).

because of the large ratio of spot size (10 μm) to expansion scale length (10 nm). We assume a nonideal adiabatic expansion from a uniformly heated target, guided by many previous numerical simulations of short-pulse laser interactions [2]. The nonideal equation of state is calculated from the Saha equation, and the rarefaction flow is given by a self-similar (Riemann) solution. We determine the dielectric function of the expanding gold by comparison to the experimental results of Fig. 3. For low-density gas, the formula $\varepsilon = 1 + 4\pi n_{\text{atom}}\alpha(\omega)$ is used, while the Drude formula is used for free electrons in the dense metal. The calculation gives $X = (R_p/R_s)$ and $Y = (I_3 - I_4)/(I_3 + I_4)$ at various times in the expansion. Figure 4 shows theoretical (X, Y) trajectories for gold targets expanding from solid density with initial temperatures of 5, 10, 15, 20, and 25 eV. This simulation reproduces most features of the experiment, especially the unique (X, Y) trajectory independent of initial temperature. For initial temperatures in this range (5–25 eV), the low-density plasma cools to temperatures below 1 eV and recombines to mainly neutral atomic gold vapor.

Finally, we can discuss some conclusions. A small fraction of free electrons in the low-density vapor can have a large effect on the X, Y trajectories. If the expanding vapor were ionized, the electron density should depend on temperature and density. However, the observed X, Y trajectories follow approximately the same curve in this intensity range. This is easily understood if the expanding vapor is mainly neutral ground state atoms. Trajectories calculated for an ionized vapor disagree with the experiment by ~10%–20%, depending on the damping time assumed (see also Ref. [8]). In experiments at higher intensity ($> 10^{14}$ W/cm^2), not presented here, the experimental X, Y points fall below the trajectory shown in Figs. 3 and 4, and probably in that case the gold does remain ionized.

We assume an atomic polarizability $\alpha(\omega) \sim (-1.75 + 0.2i) \times 10^{-24}$ cm^3, chosen to approximately match the experiments. The leading edge of the expansion, defined as the point where the fluid velocity extrapolates to zero, reaches 100–300 Å in 1 ps, corresponding to a gold atom kinetic energy of the order of 100 eV. The velocity ~10 km/s corresponds to a gold atom kinetic energy ~100 eV. This energy seems very high for neutral gold, which has a 9.22 eV ionization potential (20.5 eV for Au^+). The simulation shows that the expansion velocity is determined by the high pressure in the early stages of the expansion. As the plasma expands, its temperature falls and the electrons recombine but the expansion velocity does not decrease. Figure 5 shows a typical result of this model at 1 ps after the start of expansion. Initially, the plasma had a 5 eV temperature. (This case corresponds to a low-intensity experiment.) At about 1 ps, the low-density vapor cools into the two-phase region (temperature <0.5 eV) and may recondense.

If we represent the dielectric function for cold solid gold in terms of an atomic polarizability, we find $\alpha = (-29.7 + 0.14i) \times 10^{-24}$ cm^3, very different from the value which matches the gold vapor. This large change

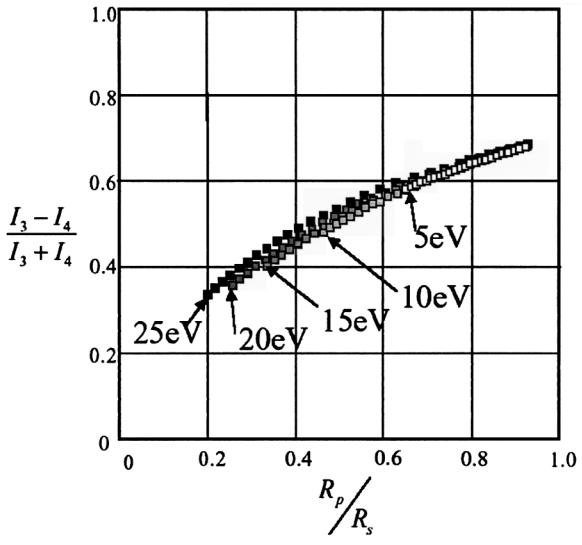

FIG. 4. Calculated gold ellipsometry trajectories. The Maxwell equation with a constant atomic polarizability for gold vapor and a Drude law for high-density gold were solved for this calculation. The cases shown are based on nonideal adiabatic rarefactions from solid gold at initial temperatures of 5, 10, 15, 20, and 25 eV. In each case the trajectory is followed for 1 psec. The cases differ mainly in the expansion velocity which controls the rate of change of the X, Y parameters, but the trajectories follow approximately the same curve in X, Y space.

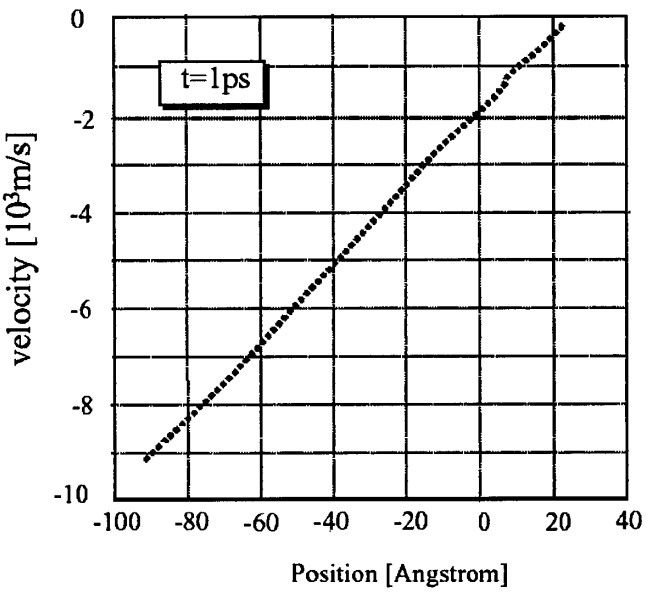

FIG. 5. The calculated velocity of gold vapor. The Saha equation and adiabatic expansion were assumed for this calculation. Although the initial temperature is not high (5 eV), expansion velocity of the front plasma can reach 10 km/s. This high velocity is created by the initial high pressure.

in optical constants and the measurement of the s-p phase shift (in the variable Y) combine to give us good sensitivity to the expansion length.

Many previous ultrashort-pulse laser experiments have been performed with aluminum targets [1,2,6,9]. For the most part, these were successfully modeled using the Drude theory for an ionized (metallic) plasma. Our experiments present special features because of the high ionization potential (9.2 eV) and strong electron affinity (2.3 eV) of neutral gold and the long probe time delays (up to 1 psec) which give the plasma time to recombine. The unique (X, Y) trajectory for ellipsometric reflection from the expanding plasma is a consequence of recombination to a unique atomic state, the neutral ground state. The model generally explains the experimental observations.

The Saha equation predicts a surprising plasma composition for the low-temperature ablation region: mostly neutral gas with a few percent positive ions balanced by negative ions and *very few free electrons*. This is a novel type of laser-produced plasma, predicted to arise when the expanding plasma cools below 0.5 eV. This prediction also helps us understand the experiments because the formation of negative ions reduces the contribution of free electrons to the dielectric constant.

[1] A. Ng *et al.*, Phys. Rev. Lett. **57**, 1595 (1986).
[2] D. F. Price *et al.*, Phys. Rev. Lett. **75**, 252 (1995).
[3] N. I. Zheludev *et al.*, Opt. Lett. **20**, 1368 (1995).
[4] S. Dhanjal *et al.*, Opt. Lett. **22**, 1879 (1997).
[5] P. Blanc *et al.*, J. Opt. Soc. Am. B **13**, 118 (1996).
[6] M. K. Grimes *et al.*, Phys. Rev. Lett. **82**, 4010 (1999).
[7] E. Collett, Surf. Sci. **96**, 156 (1980).
[8] M. Desjarlais, Contrib. Plasma Phys. **41**, 267 (2001).
[9] H. M. Milchberg *et al.*, Phys. Rev. Lett. **61**, 2364 (1988).